

Wind tunnel section model study of aeroelastic performance for Ting Kau Bridge Deck

James Mark William Brownjohn[†] and Cheong Chuen Choi[‡]

School of Civil and Structural Engineering, Nanyang Technological University, 50 Nanyang Avenue, Singapore 639798, Singapore

Abstract. Wind tunnel tests were conducted on a model of deck section from the Ting Kau cable stayed bridge. The purpose of the tests was to determine the set of aerodynamic derivatives conventionally used to describe the motion-induced forces arising from the wind flow, and to investigate the stability of the deck under different conditions of turbulence and angle of attack. The study shows that except for large negative angles of attack the deck section itself is stable up to a high wind speed, and that when instability does occur it is essentially a single degree of freedom (torsional) flutter.

Key words: cable-stayed bridge; wind tunnel; section model; flutter derivatives.

1. Introduction

For cable-supported bridges, because of the high degree of flexibility, bridge movements i.e., deflection and acceleration are of primary concern in the design of the bridge. The motion of the bridge is not just caused by wind; the motion in wind leads to dynamic forces. Such motion-induced forces play a very important role with cable supported bridges since under certain condition the energy derived from the motion induced loads can exceed the energy dissipated by structural damping. Unlike vortex shedding which has limited amplitude, this instability (like galloping) has unlimited amplitude as long as the structure properties remain linear and is conventionally called flutter, whether it is a single degree of freedom (torsion) or coupled (torsional/vertical) motion.

2. Ting Kau Bridge

The Ting Kau Bridge (King, Davenport and Schlaich 1997) with its 1177 m length is one of the longest cable-stayed bridges in the world. It consists of two main spans of 448 m and 475 m and two side spans and provides a vital link in Hong Kong's new Route 3, connecting Hong Kong Island, Kowloon and the new airport on Lantau to the New Territories and the border to Mainland China. It is supported on three piers, one at Tsing Yi, one at Ting Kau and the third on an artificial island. The deck has a varying chord with a minimum of 42.8 m excluding fairings, and is separated into two carriageways. Each carriageway has a camber of approximately 2.5% with two longitudinal L-shaped edge girders, and I-shaped cross beams every 4.5 m. Every 13.5 m cross beams extend to

[†] Associate Professor

[‡] Professor

connect with the other carriageway across a 5.26 m void. The deck is very slender with a very high chord to depth ratio (approximately 25) making it potentially susceptible to aerodynamic actions. Since the bridge is situated in a typhoon area it will during its lifetime be subject to very strong winds. It is thus important to establish the relationship between wind actions and bridge response. Furthermore, because of its slender section and bluff edges the aerodynamic stability is of great concern.

Aerodynamic and aeroelastic studies to determine the best shape of section were originally carried out at BLWTL Ontario (Bergemann and Schlaich 1996) and a set of tests on behalf of Highways Department through Hong Kong University (HKU) and South China University (SCU) was carried out at NTU Singapore. These tests were done to extract aerodynamic derivatives (flutter derivatives) for HKU/SCU to simulate the bridge performance via numerical models.

3. Wind tunnel studies and aerodynamic derivatives

Since the spectacular collapse of the Tacoma Narrows Suspension Bridge (Wyatt 1992) due to wind-induced instability, wind tunnel section model tests, in which a geometrically and aerodynamically representative scale model of a length of a bridge deck is mounted in a wind tunnel, have been a major tool in studying the wind effects on a bridge deck. As well as identification of static force coefficients, section models can be used to study the effects of motion-induced forces and instability or flutter. The motion-induced forces can be obtained either by direct measurement (Scanlan and Tomko 1971, Bogunovic-Jakobsen 1995) or by their effect on the dynamic performance of a model which is allowed to oscillate with one or two degrees of freedom i.e., vertically or torsionally. The motion-dependent forces feed back into the dynamics of the bridge as aerodynamic damping and stiffness and the effect is termed 'aeroelasticity' and described via coefficients or aerodynamic derivatives (Scanlan and Sabzevari 1969) (ADs) or 'flutter derivatives' which are non-dimensional functions of wind speed, geometry and frequency of oscillations.

Identification of the ADs is a vital step in performance predictions for a wind-sensitive full-scale structure. Being non-dimensional functions only of the shape of the section they can be applied directly to full-scale through modal integrals.

Various methods are used to extract the ADs from wind tunnel tests on geometrically and aerodynamically representative models. From the experimental point of view the simplest technique is to obtain and analyse free vibration response records (Scanlan and Sabzevari 1969). The model is suspended by springs from a rigid test frame and will vibrate freely in response to a transient deflection (step relaxation) or to buffeting caused by the airflow turbulence.

4. Test arrangement for free vibration response

Fig. 1 shows the schematic arrangement of a length L of bridge section model in a wind tunnel with horizontal incident wind having mean speed U . The deck has chord B , total mass m_T and total moment of inertia I_T about the geometric centreline. The section is attached to a rigid test frame at each corner by linear springs with stiffness k arranged at distance e upstream or downstream of the geometric centreline. The contributions of spring mass to total mass and inertia are accounted for by adding $1/3$ of their mass at their point of attachment. Vertical and torsional displacements and their time-derivatives at mid-chord are respectively denoted $h, \dot{h}, \ddot{h}, \theta, \dot{\theta}, \ddot{\theta}$ and are related to acceleration values \ddot{y}_1, \ddot{y}_2 at points close to leading and trailing edges of the section, at separation c . Vertical and torsional accelerations can be obtained from the sum and difference of edge accelerations :

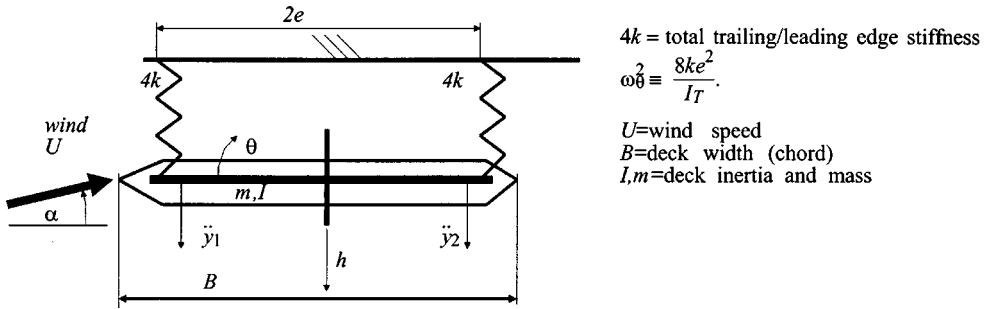


Fig. 1 Schematic of deck section test configuration showing parameters and conventions

$$\ddot{h} = (\ddot{y}_1 + \ddot{y}_2)/2, \quad \ddot{\theta} = (\ddot{y}_2 - \ddot{y}_1)/c$$

In still air without aerodynamic influence the natural frequencies of the deck for rigid body vibration are in theory obtained as

$$f_{\theta} = (1/2\pi)\sqrt{k_{\theta}/I_T} \text{ and } f_h = (1/2\pi)\sqrt{k_h/m_T} \text{ where } k_{\theta} = 8ke^2 \text{ and } k_h = 8k.$$

In practice the test rig and model do not present exact rigid body modes and there may be a degree of torsion or bending present in the model.

5. Choice of structural/geometric parameters for section test

The scale ratio for the model was kept to a minimum to allow for adequate detailing in construction while leaving a span to chord ratio L/B of at least 3. A length scale of 1:80 was chosen giving a model chord $B = 0.574$ m, including fairings for $L = 1.527$ m representing 121.6 m of deck with 10 cross beams at ends and equal intervals.

For a wind tunnel maximum working wind speed $\hat{U} = 20$ m/sec the spring rates and separation k and e are chosen to obtain a range of non-dimensional wind speeds U/fB consistent with prototype values of f and design wind speed. The prototype has a vertical mode frequency estimated as 0.174 Hz. Note: the design hourly mean speed (at deck level) is 50 m/sec and the design 3-second gust wind speed (at deck level) is 80 m/sec. The model vertical mode frequency f_h is then set via :

$$(U/f_h B)_{prototype} \approx 10.7 \approx (\hat{U}/f_h B)_{model} \text{ i.e., } f_h = 3.25 \text{ Hz, with similar factors applying to } f_{\theta}.$$

Appropriate materials are used to achieve geometric accuracy with adequate stiffness to prevent occurrence of the low frequency deformation modes in the model. Given the resulting model mass the spring rate k can be chosen to achieve f_h . Spring separation can be adjusted to control f_{θ} .

The set of vertical springs does not restrain lateral or longitudinal deflections or rotation about a vertical axis. Drag wires are installed to resist but not entirely constrain these motions. Practical issues relating to set up of section model tests are well documented by Hjorth-Hansen (1992).

6. Details of section model and test rig

6.1. Section model

Fig. 2 shows plan and end elevation of the section model, although the elevation does not show

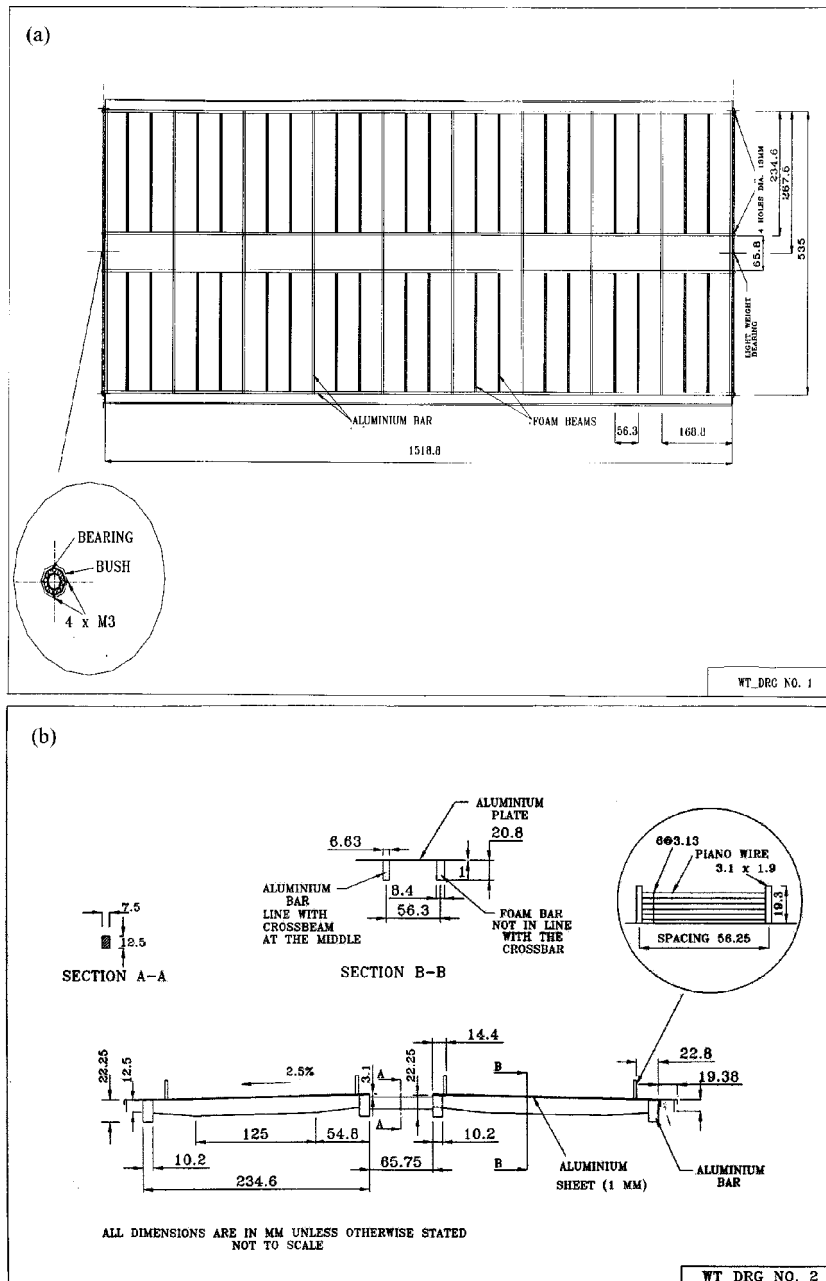


Fig. 2 Section model (a) plan view (b) end elevation

the presence of the skirt added to leading and trailing edges for the testing. In the construction of a section model, on the one hand, strong material has to be used so that the model can be very stiff to simulate a rigid prototype bridge section. On the other hand, It is also necessary for the model to stimulate the mass density and the mass distribution of the prototype which demands the use of relatively light material. Aluminium was chosen to be the main material for model construction. The longitudinal girders and the main cross girders were constructed with aluminium sections. The bridge deck was constructed with aluminium plate. Secondary cross girders are constructed using high density styrofoam to make up for the shape.

The model and suspension was entirely contained in the wind tunnel and no end plates were used. The issue of using end plates is discussed by Hjorth-Hansen (1992) and it is reasonable that for span/chord ratios of 5 and above end plates may not be necessary. For this model the ratio was only 3 but it was decided to trade one kind of end effect for another and benefit from a simple test arrangement.

6.2. Mounting frame

A mounting system was constructed where the model was suspended by four springs at each end. The springs were so chosen such that they have a combined stiffness producing the desirable frequencies of vibration of the model. The anchor points of the springs are fixed on slides that enable the spring positions to be changed as required. The initial tension in the springs can be adjusted by varying the distance between the anchor bars. A bearing is also installed so that the model can rotate about its central axis. Drag wires can be tied to various locations of the model support which allows the model motion to be either solely in the vertical direction or solely rotational about the central axis or coupled vertical and rotational. This setup enables the experiment to be carried out such that vertical and torsional modes of vibration can be isolated or coupled. The frequencies of vibration of the model can also be controlled to be in a range of magnitudes similar to that of the prototype. Fig. 3 show the setup of the experiment.



Fig. 3 Section model and test rig

7. Aeroelasticity and identification of aerodynamic derivatives

For identification of all eight derivatives involving only vertical and torsional motion, the equations of motion for a 2DOF section with length L and width B , in air flow with density ρ and speed U according to the conventions of Fig. 1, are :

$$m_T \ddot{h} + c_h \dot{h} + k_h h = \frac{\rho U^2 B L}{2} \left[h_1 \frac{\dot{h}}{U} + h_2 \frac{B \dot{\theta}}{U} + h_4 \frac{h}{B} + h_3 \theta \right] + L_{buf} \quad (1)$$

$$I_T \ddot{\theta} + c_\theta \dot{\theta} + k_\theta \theta = \frac{\rho U^2 B L}{2} \left[a_1 \frac{B \dot{h}}{U} + a_2 \frac{B^2 \dot{\theta}}{U} + a_4 h + a_3 B \theta \right] + M_{buf} \quad (2)$$

On the left hand side the mechanical damping coefficients are c_h, c_θ for each DOF. The right hand sides are aerodynamic lift and moment forces L_{ae}, M_{ae} which depend on non-dimensional coefficients or aerodynamic derivatives (ADs). The ‘direct derivatives’ h_1, h_4, a_2, a_3 represent effects within a single DOF response while ‘cross-derivatives’ h_2, h_3, a_1, a_4 represent coupling between the DOF. Buffeting lift and moment forces are denoted L_{buf}, M_{buf} respectively.

An alternative form for aerodynamic lift and drag forces uses ADs which are frequency dependent coefficients :

$$L_{ae} = \rho U^2 B L \left[K H_1^*(K) \frac{\dot{h}}{U} + K H_2^*(K) \frac{B \dot{\theta}}{U} + K^2 H_3^*(K) \theta + K^2 H_4^*(K) \frac{h}{B} \right] \quad (3)$$

$$M_{ae} = \rho U^2 B^2 L \left[K A_1^*(K) \frac{\dot{h}}{U} + K A_2^*(K) \frac{B \dot{\theta}}{U} + K^2 A_3^*(K) \theta + K^2 A_4^*(K) \frac{h}{B} \right] \quad (4)$$

Note that there are different forms (Zasso 1996) of Eqs. (3) and (4) using for example the half-chord $B/2$ as reference instead of B and using $\rho U^2 B L / 2$ instead of $\rho U^2 B L$. Simple algebraic relations such as $h_1 = 2KH_1^*(K)$ link the A_i^*, H_i^* in Eqs. (3) and (4) to the a_i, h_i in Eqs. (1) and (2) where $K = B\omega / U = 2\pi f B / U$ is the reduced frequency.

7.1. Single Degree of Freedom (SDOF) tests and identification

ADs can be identified from SDOF tests in which one DOF is restrained or from 2DOF tests when torsional and vertical motion is allowed. For example if torsion is restrained using an arrangement of drag wires, Eq. (1) reduces to

$$m_T \ddot{h} + c_h \dot{h} + k_h h = \frac{\rho U^2 B L}{2} \left[h_1 \frac{\dot{h}}{U} + h_4 \frac{h}{B} \right] + L_{buf} \quad (5)$$

If the section is pulled down (e.g., by wire through the floor of the wind tunnel) and released, the solution for free vibration (transient) decay from initial deflection h_o is

$$h(t) = h_o e^{\lambda t} \cos(\omega t + \phi) \quad (6)$$

In a wind stream with velocity U and vertical response given by Eq. (6), the direct vertical derivatives h_1, h_4 hence H_1^*, H_4^* are found from the shifts in λ, ω given by :

$$-\lambda = \xi_h \omega_h - \frac{\sigma U B L h_1}{4 m_T} \quad \text{and} \quad \omega^2 = \frac{k_h}{m_T} - \frac{\rho U^2 L h_4}{2 m_T} \quad (7)$$

hence the identification of H_1^* , H_4^* is thus relatively straightforward. Similarly A_2^* , A_3^* can be found if vertical motion is restrained.

7.2. Two Degree of Freedom (2DOF) tests and identification

The pair of equations of motion (1) and (2) may be rewritten in matrix form :

$$\mathbf{M}\ddot{\mathbf{z}} + \mathbf{C}_{str}\dot{\mathbf{z}} + \mathbf{K}_{str}\mathbf{z} = \mathbf{C}_{ae}\dot{\mathbf{z}} + \mathbf{K}_{ae}\mathbf{z} + \mathbf{p}(t) \quad (8)$$

where \mathbf{M} represents mass terms, \mathbf{C} represents structural or aerodynamic damping terms and \mathbf{K} represents structural or aerodynamic stiffness terms. Vectors of measurable response and of buffeting load are

$$\mathbf{z} = \begin{bmatrix} h \\ \theta \end{bmatrix}, \quad \mathbf{p} = \begin{bmatrix} L_{buf} \\ M_{buf} \end{bmatrix} = \begin{bmatrix} g_h \\ g_a \end{bmatrix} u(t)$$

The buffeting input is represented by a common (wind dependent) forcing function $u(t)$ and two gain factors g_h , g_a which depend on mean wind speed, section shapes and static aerodynamic coefficients.

Eq. (8) can be rewritten in 'state space' form :

$$\begin{aligned} \dot{\mathbf{x}} &= \mathbf{A}\mathbf{x} + \mathbf{B}u \\ \mathbf{y} &= \mathbf{C}\mathbf{x} + \mathbf{D}u \end{aligned} \quad (9)$$

with initial values $\mathbf{x}_o = [h \ \dot{h} \ \theta \ \dot{\theta}]'$.

For the case of free vibration due to an initial deflection, MATLAB (1998) system identification routines can be used to identify the values of \mathbf{A} and \mathbf{x}_o for which the time histories generated using Eq. (8) give the best match to the observed data. Some system identification methods used in the study are presented elsewhere (Brownjohn and Bogunovic-Jakobsen).

8. Test program

The wind tunnel testing was done in two phases :

- Phase 1: Identify the set of eight direct and cross derivatives via SDOF and 2DOF tests in smooth flow for zero angle of attack and study stability for different ratios of torsional to vertical frequency. Identification methods described above were used.
- Phase 2: Identify derivatives in turbulent flow and with non-zero angles of attack. Identification methods described above were used together with methods for analysing free vibration response to turbulent buffeting.

8.1. Smooth flow SDOF tests at zero angle of attack

Torsional SDOF tests were done first for 'smooth flow' i.e., with turbulent intensity I less than 3%, for zero angle of incidence α and with spring separation e set to 0.504 m for maximum torsional frequency i.e., $f_\theta = 5.135$ Hz. Fig. 4 shows examples of response (a) 'in still air' and (b) 'in wind' with vertical motion restrained to identify the direct torsional direct derivatives A_2^* , A_3^* . Fig. 5 shows the change in frequency and the total damping ratio and the derived ADs, plotted against non-dimensional (reduced) wind speed U/fB , f being the frequency of the still air SDOF

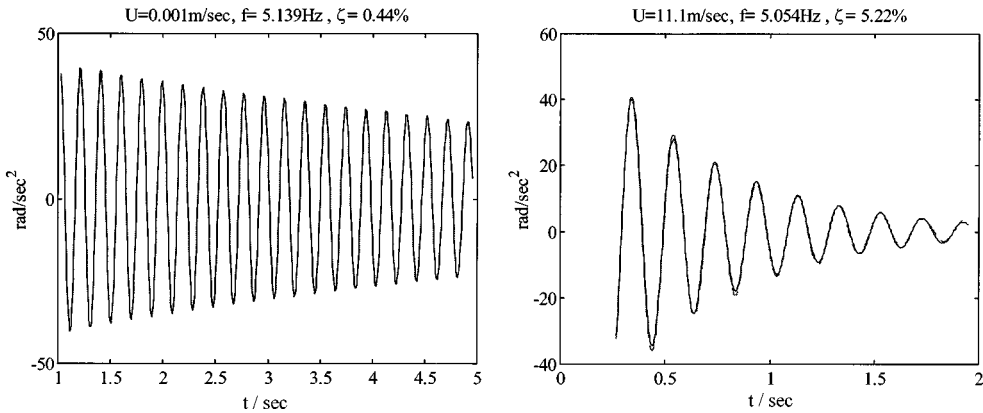


Fig. 4 Torsional free vibration decay of section in still air (above) and in wind (below)

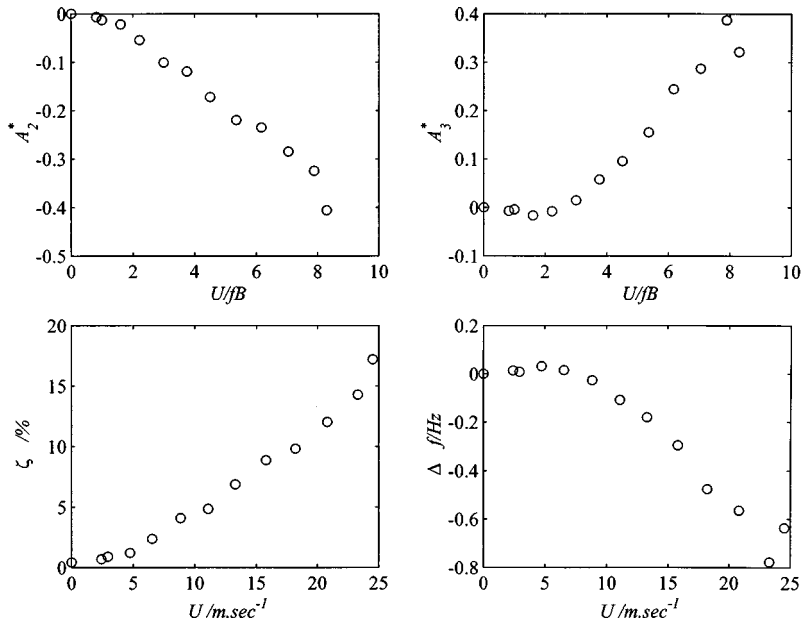


Fig. 5 Damping ratios, frequency shifts and direct derivatives for torsional response in smooth flow at zero angle of attack

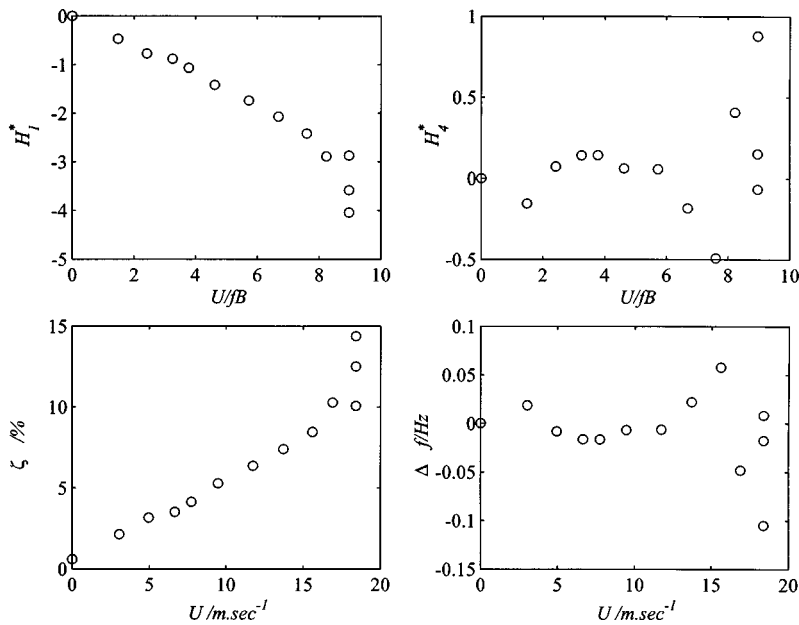


Fig. 6 Damping ratios, frequency shifts and direct derivatives for vertical response in smooth flow at zero angle of attack

motion.

Up to about $U = 8$ m/sec the frequency increases slightly then decreases steadily. At the same time the damping increases steadily so there can be no SDOF instability in these conditions. The same values and patterns of A_2^* , A_3^* are obtained using a different e to reduce torsional frequencies.

Vertical SDOF tests were then done with restraint on torsional motion provided by an arrangement of drag wires attached to upper and low ends of a vertical torsion bar (Fig. 1) and with a ‘still air’ vertical frequency $f_h = 3.569$ Hz. Fig. 6 shows the trends in frequency and damping and the resulting direct derivatives H_1^* , H_4^* . For damping the increases is clear and strong, hence there is no risk of SDOF instability with vertical motion (galloping). For the frequency data, there is increasing scatter in frequency estimates with no clear trend.

The data described above were obtained from free vibration decay. One problem with the testing is the increase in signal noise with increased wind speed. For example the turbulent buffeting response can be stronger than the free decay that can be induced by pulling and releasing. Also, even with restraints against other DOF and cancellation of other DOF signals by sum and difference of edge response there is some contamination, hence selection of a representative free decay signal becomes increasingly difficult for high wind speeds.

8.2. Smooth flow 2DOF tests at zero angle of attack

The cross derivatives which would be responsible for classical 2DOF flutter were evaluated by system identification of the \mathbf{A} matrix in Eq. (9) through matching of time histories obtained from free vibration decay of the section. The free decay was obtained with no restraint on torsional or vertical motion, after deflecting the trailing edge of the section to induced response in both DOF. As

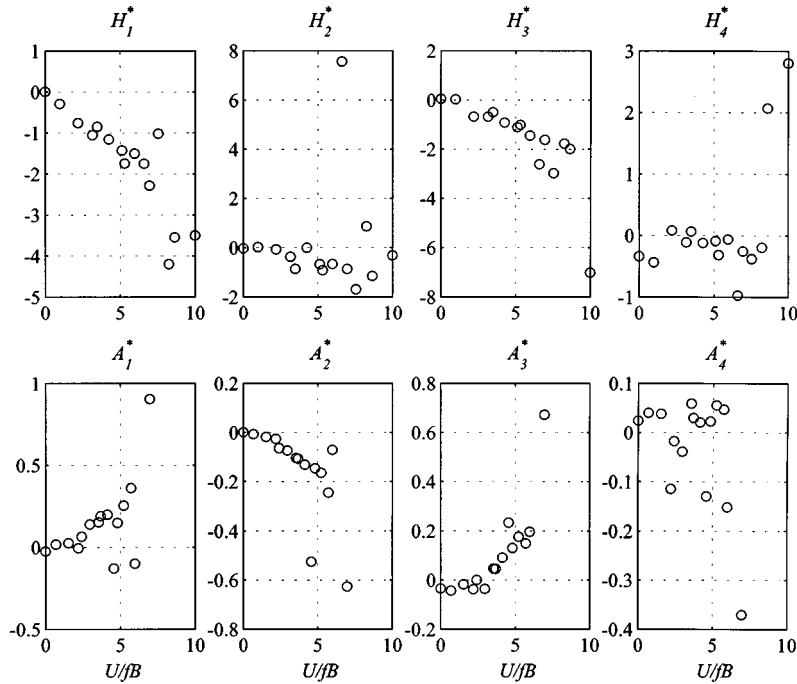


Fig. 7 Full set of aerodynamic derivatives for smooth flow and zero angle of attack

for SDOF response, obtaining a valid decay trace became increasingly difficult with the higher wind speeds, but Fig. 7 shows the full set of eight derivatives obtained by this method. Apart from the scatter, the trends for direct derivatives are consistent with those from the SDOF tests. For Fig. 7 the convention for the reduced wind speed is to use for frequency f the still air value of f_h for the H_i^* and of f_θ for the A_i^* .

8.3. Investigation of large amplitude motion and instability

While not directly applicable to the full-scale structure because of the different relationship between torsional and vertical frequencies and the averaging effect through modal integrals, some direct indication of the stability of the section is available from model studies.

For three different spring separations and three corresponding still-air torsional frequencies, the unrestrained 2DOF response was observed as wind speeds were steadily increased until the occurrence of sustained (or divergent) large amplitude oscillations of the form :

$$h(t) = h_o \cos(2\pi f_c t + \phi) \qquad \theta(t) = \theta_o \cos(2\pi f_c t)$$

Table 1 summarises the conditions for each case in terms of :

- Still air torsional frequency f_θ ,
- Still air frequency ratio f_θ / f_h ,
- In-wind frequency for oscillations f_c ,

Table 1 Large amplitude/divergent oscillations

Spring separation e / m	Still air torsional frequency f_{θ} / Hz	$U_{crit} / m.sec^{-1}$	In-wind frequency f_c / Hz	Reduced velocity $U / f_c B$	Frequency ratio f_{θ} / f_h	$h_o / \theta_o / m.radian^{-1}$	$\phi / degree$
0.24	2.675	17	2.97	9.95	0.755	0.096	146
0.32	3.391	20	3.63	9.58	0.963	0.702	107
0.504	5.142	25	4.70	9.25	1.44	0.432	39

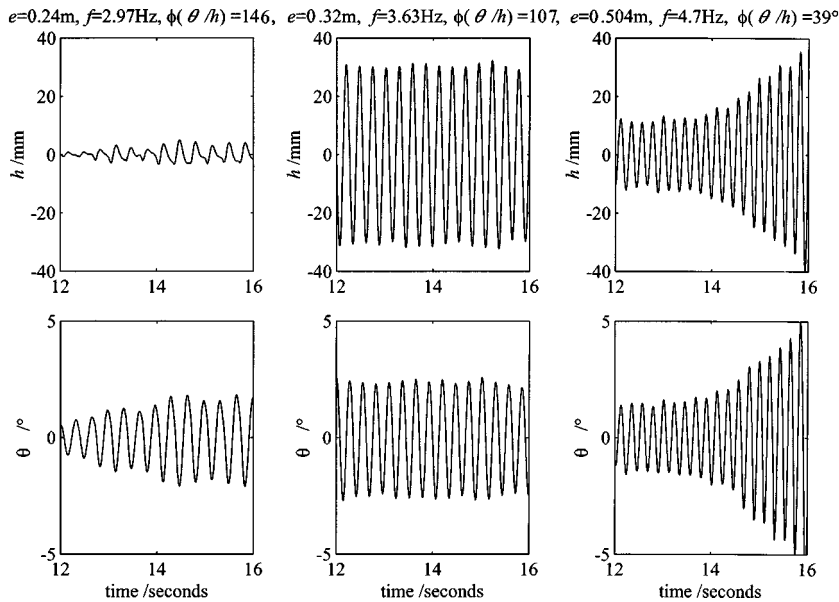


Fig. 8 Two degree of freedom free vibration response at critical wind speeds for different spring separations (e) and corresponding still air torsional frequencies

- Critical wind speed U_{crit} ,
- In-wind reduced velocity $U / f_c B$
- In-wind amplitude ratio h_o / θ_o and
- Relative phase angle ϕ

The oscillations are shown in Fig. 8 as mm and degrees; the model chord is 574 mm and 1° inclination gives a 9.55 mm relative height between trailing and leading edges. For the first two conditions the small spring separation and weak torsional stiffness led to noticeable negative angle of attack (dip of leading edge) due to the static moment coefficient and the oscillations resulted in slackening of lower leading and upper trailing springs. This non-linear response probably prevented the divergence that occurred for the (torsionally) stiffest condition with maximum spring separation. In each case the torsional response dominated in what was essentially SDOF (torsional) flutter. Referenced to the in-wind oscillation frequency the instability occurs for $U / f_c B$ around 9.5. Referenced to the still air value torsional frequency (which is more accessible) the reduced velocity ranges from 8 to 11.

8.4. Smooth flow SDOF tests at varied angle of attack

From the above measurements one clear factor in the aeroelastic response appeared to be angle of attack. This had also been identified by separate wind tunnel tests for the same bridge (King, Davenport and Schlaich 1997). The SDOF tests were repeated for angles of attack :

$$\alpha = -10^\circ, -5^\circ, 0^\circ, +5^\circ, +10^\circ.$$

For torsional SDOF response with still air frequency 5.3 Hz, negative angles of attack result in large amplitude oscillation at wind speeds that decrease with increasing angle of attack. Fig. 9 shows the effect for negative angles of attack compared to the neutral condition in which the solid line is fitted to the SDOF data of Fig. 5. Damping initially increases more steeply but becomes negative at 14 m/sec ($U/fB = 4.6$, for $\alpha = -5^\circ$) and at 10 m/sec ($U/fB = 3.3$, for $\alpha = -10^\circ$) with resulting large amplitude oscillation. without introducing extra structural damping (Hjorth-Hansen 1992) the curves cannot be extended. For positive angles of attack the derivatives are similar to the neutral condition with no apparent instability up to 22 m/sec ($U/fB = 7.2$).

For vertical response with still air frequency 3.7 Hz, Fig. 10 shows there is no apparent difference between the derivatives for different angles of attack and, as for the first set of tests, no clear trend in vertical frequency with wind speed. For negative angles of attack, despite the torsional restraints which acted to increase torsional frequency to 7.7 Hz, strong torsional response was observed above wind speeds of 20 m/sec ($U/fB = 4.5$, for $\alpha = -5^\circ$) and 14 m/sec ($U/fB = 3.2$, for $\alpha = -10^\circ$) consistent with the observations from torsional vibration.

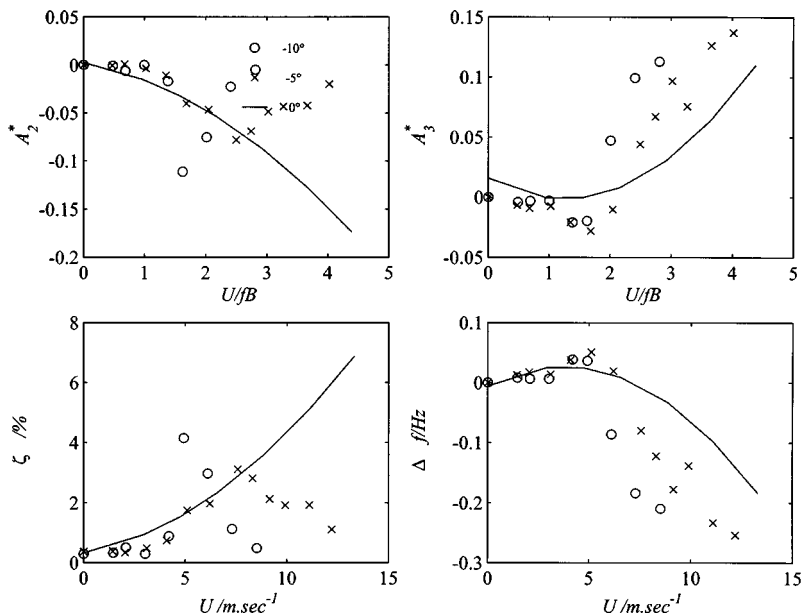


Fig. 9 Damping ratios, frequency shifts and direct derivatives for torsional response at zero angle of attack and two negative angles of attack, in smooth flow

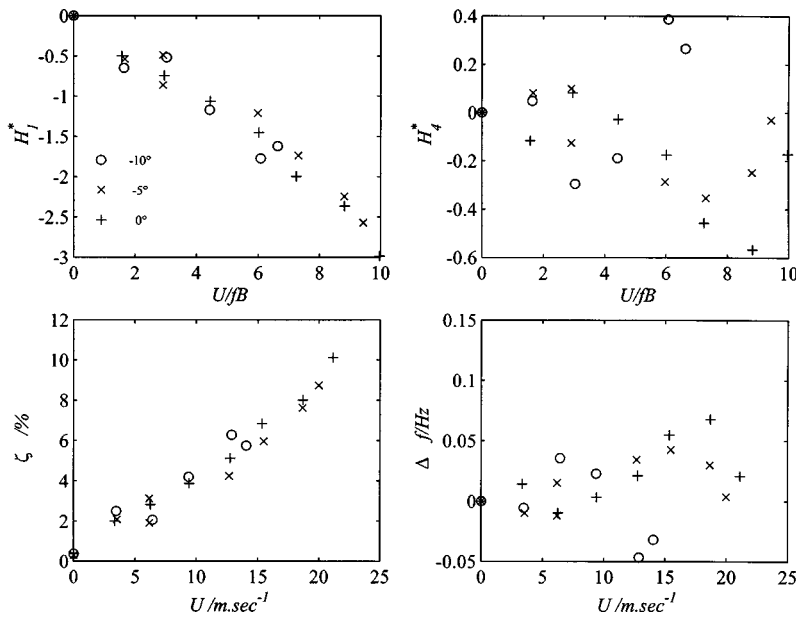


Fig. 10 Damping ratios, frequency shifts and direct derivatives for vertical response at zero angle of attack and two negative angles of attack, in smooth flow.

8.5. Turbulent flow SDOF tests

The above tests were also run with ‘low turbulence’ i.e., $I \approx 8\%$ compared to 1-3% for ‘smooth flow’. This compares to values of 10% and 16% for low and high turbulence used in other wind studies and while on the low side is sufficient to provide information about the effects of turbulence. For these tests it was not possible to estimate frequency and damping (hence derivatives) from the free vibration decay since the buffeting response exceeded the decay for all but the lowest wind speeds.

Since the buffeting response was strong it was natural to analyse the buffeting response signals. There are several methods for doing this from the time series e.g., through the autocorrelation function. Alternatively, frequency domain methods could be used through fitting the power spectra of vertical or torsional response to the response to a SDOF oscillator to a random lift or moment forcing function with flat power spectrum. For vertical response spectrum S_{hh} is related to lift spectrum S_{ll} through the expression

$$S_{hh}(\omega) = \frac{S_{ll}}{k_h^2(1 - (\omega/\omega_{h'})^2)^2 + (2\xi_{h'}\omega/\omega_{h'})^2} \quad (10)$$

where $\omega_{h'}$, $\xi_{h'}$ are in-wind frequency and damping ratio, differing from still air values.

Using this expression and the equivalent for torsional response, the frequency and damping changes were found for torsional and vertical response in the two flow conditions and are shown in Figs. 11 and 12 for zero angle of attack. The values are similar. One observation from the vertical response is the clear trend in vertical frequency and H_4^* which is not seen with the free decay data.

Fig. 13 shows effect of turbulence on the instability for negative angle of attack $\alpha = -5^\circ$.

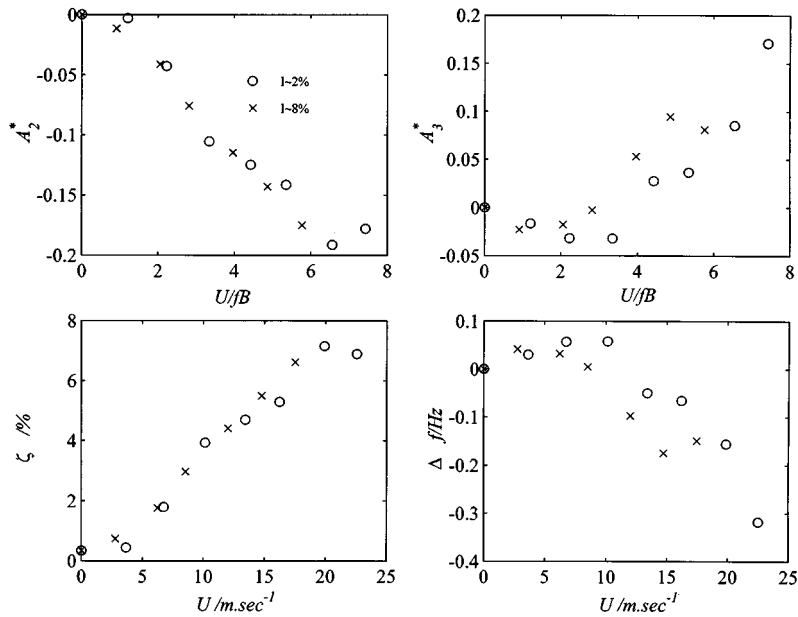


Fig. 11 Damping ratios, frequency shifts and direct derivatives for torsional response at zero angle of attack in smooth flow and turbulent flow

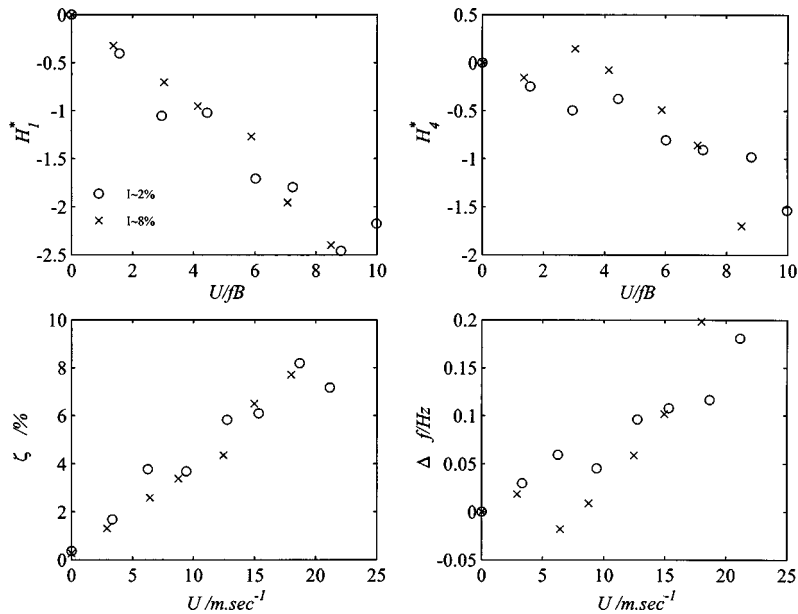


Fig. 12 Damping ratios, frequency shifts and direct derivatives for vertical response at zero angle of attack in smooth flow and turbulent flow

Turbulence has only a minor effect (if any) on the torsional response. The data were obtained from the frequency response analysis.

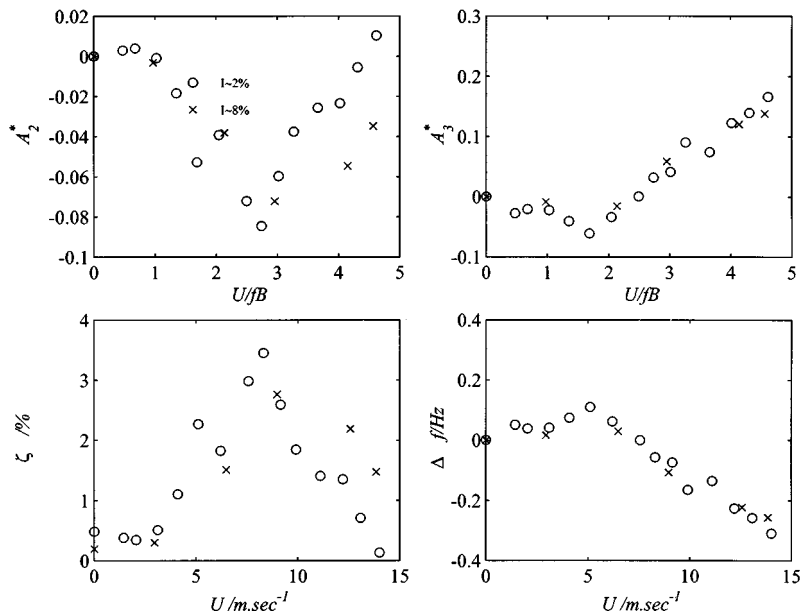


Fig. 13 Damping ratios, frequency shifts and direct derivatives for torsional response at -5° angle of attack in smooth flow and turbulent flow

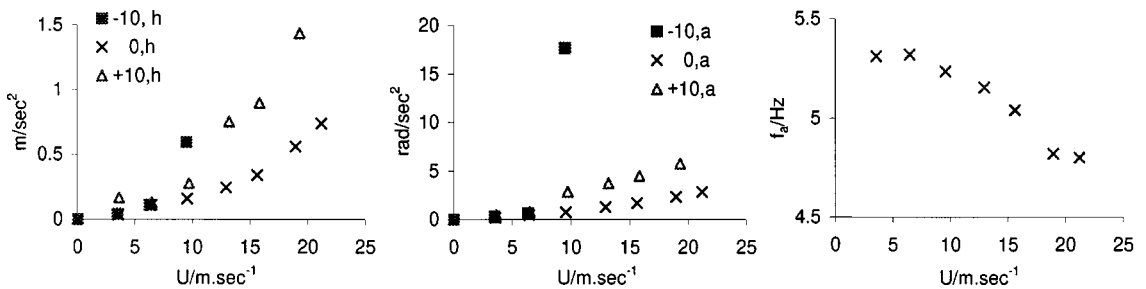


Fig. 14 RMS vertical and torsional response amplitude in smooth flow for different angles of attack (above), and torsional frequency shifts for zero angle of attack (below)

8.6. 2DOF tests for varied angle of attack

A small number of tests were done in which the 2DOF buffeting response of the section was observed with neither torsional nor vertical restraints. For these tests the RMS response values were measured for a range of wind speeds with three angles of attack $\alpha = -10^\circ, 0^\circ, +10^\circ$. These values are shown in Fig. 14 together with values of torsional frequency $f_a = f_\theta$ for neutral condition. The negative damping effect for negative angle of attack is clear.

9. Conclusions

The tests clearly demonstrate the stability of the section as built with the fairings and its dependence on angle of attack. Torsional instability is observed for U/fB exceeding 8 for the neutral condition

(zero angle of attack), decreasing to 4.5 for -5° and 3.3 for -10° . For positive angles of attack the stability is little changed from the neutral condition. For the high torsional natural frequency of the prototype, believed to be 0.4 Hz, these correspond to full-scale wind speeds of 147 m/sec, 83 m/sec and 61 m/sec respectively. Since large negative angles of attack are very unlikely to be sustained the instability should never be an issue.

As for test methods, conventional free decay analysis techniques were successful for direct derivative estimation in smooth flow conditions and 2DOF system identification was successful. For turbulent flow the methods cannot be used so easily and methods such as the eigensystem realisation algorithm that work well with ‘ambient vibration’ response should be used. One problem in the data reduction is noise from instruments and higher structural vibration modes. Relatively low grade accelerometers were used with filtering (and integration where necessary) to recover time histories. Direct measurement of displacement signals by optical methods coupled with ambient vibration identification techniques improves parameter estimation techniques.

Acknowledgements

The section model tests were conducted as part of a collaborative research project between NTU, University of Hong Kong and South China University of Technology and funded by Hong Kong Highways Dept.

The authors are grateful to Ms. Sally Aw and Mr. Tay Lye Chuan for wind tunnel operations, Prof. Alberto Zasso (Politecnico di Milano) for direction in the 2DOF identification methods and Prof. Erik Hjorth-Hansen for direction in the experimental set up.

References

- King, J. P. C, Davenport , A. G. D. and Schlaich, M. (1997), “Wind engineering studies for the Ting Kau Bridge, Hong Kong”, *Building to Last. Proc. of ASCE Structures Congress XV*, **1**, 175-179.
- Bergemann R. and Schlaich, M. (1996), “Ting Kau Bridge, Hong Kong”, *Structural Engineering International*, (IABSE) No. 3, 52-154.
- T. A. Wyatt, T. A. (1992), “Bridge aerodynamics 50 years after Tacoma Narrows - part 1: The Tacoma Narrows failure and after”, *J. Wind Eng. Ind. Aerod.*, **40**, 317-326.
- R. H. Scanlan, R. H., and Tomko, J. J. (1971), “Airfoil and bridge deck flutter derivatives”, *J. Eng. Mech.*, ASCE EM6, **97**, 1717-1737.
- Bogunovic-Jakobsen, J. (1995), “Fluctuating wind load and response of a line-like engineering structure with emphasis on motion-induced wind forces”, *Doktor Ingeniøravhandling*, NTH 1995:62, Department of Structural Engineering, Norwegian Institute of Technology, University of Trondheim, Norway.
- R. H. Scanlan, R. H. and Sabzevari, A. (1969), “Experimental aerodynamic coefficients in the analytical study of suspension bridge flutter”, *J. Mech. Eng. Science*, **11**, 234-242.
- Hjorth-Hansen, E. (1992), “Section model tests”, *Aerodynamics of Large Bridges*, Balkema 95-112.
- Zasso, A. (1996), “Flutter derivatives: Advantages of a new representation convention”, *J. Wind Eng. Ind. Aerod.*, **60**, 35-47.
- “Using MATLAB Version 5”, (1998), *The Mathworks*, USA.
- Brownjohn, J.M.W. and Bogunovic Jakobsen, J. “Strategies for aeroelastic parameter identification from bridge deck free vibration data”, *J. Wind Eng. Ind. Aerod.*, (in press).